THE EXPERIMENTAL ULTRAFAST

MAGNETO-OPTICAL KERR EFFECT

A thesis submitted in partial fulfillment of the requirements
for the degree of Bachelor of Science with Honors in
Physics from the College of William and Mary in Virginia,

by

Jennifer Ann Wilkes

Accepted for _____

(Honors, High Honors, or Highest Honors)

_____
Dr. Anne Reilly, Advisor

_____
Dr. Keith Griffioen

_____
Dr. Gina Hoatson

_____
Dr. Sarah Stafford

_____
Dr. Michael Trosset

Williamsburg, Virginia

April 2000

Acknowledgements

A single page in a paper seems paltry homage, indeed, to pay to those individuals who have given their continual support to me over the course of the past academic year. First and foremost, thank you Anne for all of the guidance you have given me, above and beyond the call of duty. Thank you for the patience you have shown in repeatedly explaining concepts and phenomena from different perspectives until I finally "get it," and for always making time for me in your already-full schedule. I have learned a tremendous amount from you this year! Thank you Jason, Julie, and John for your technical and moral support in the lab; I never would have gotten the laser mode-locked, my broken springs soldered, or all those buttons figured out if it hadn't been for your combined expertise. Thank you Keith Griffioen, Gina Hoatson, Sarah Stafford, and Michael Trosset for taking the time out of your schedules during a hectic time of year to read my thesis and sit on my committee. And finally, thank you Lisa for your support and sense of humor that kept me going through the frustrating weeks of elusive data and those long nights of computer crises.

Abstract

An experimental setup, designed to study the magnetization characteristics of magnetic thin films by utilizing the magneto-optical Kerr effect, is constructed. Linear methods are investigated as a means of studying static magnetization properties of a sample. Nonlinear methods are investigated as a means of studying the time dependence of induced changes in the magnetization properties of a sample. Various detection schemes are explored. Data are taken for single-layer and exchange-biased multilayer thin films.

List of Figures

Table of Contents

I Introduction

Technology has come to play an ever-widening role in our day to day lives. The quest for smaller, faster computers serves as a driving force behind current scientific research. At present, the limiting factor is the speed at which data can be accessed. Information on hard drives is stored in non-volatile magnetic bits, and the process of reading data involves measuring the difference in the magnetic field between encoded ones and zeros. As the read head passes over magnetic bits, a tiny magnetic layer in the read head flips back and forth, aligning itself with the underlying bit's magnetic field. Due to the properties of the magnetic multilayer in the read head, the read head experiences a change in resistance (known as giant magnetoresistance), which provides a signal for reading the bits. The time required to write and read the magnetic bits is limited to a few nanoseconds because of limitations on the electronics used in these devices. Since this time scale determines the drive's processing speed, it is of fundamental technological importance. New methods of reading and writing data are therefore being investigated in an attempt to further increase processing speeds.

One key difficulty in this quest is the relatively poor understanding of the dynamic properties of magnetic materials we have at present, particularly our poor understanding of the time scale of domain formation in ferromagnetic materials. For example, we would like to gain a better understanding of the time required for atoms to settle back into a ferromagnetic domain after a ferromagnet has momentarily been heated above its Curie temperature (so as to demagnetize

the material), as well as a better understanding of the material's changing magnetic properties during this settling time. The purpose of this thesis work is to build an ultrafast pump-probe apparatus that utilizes the magneto-optical Kerr effect in an attempt to achieve picosecond ($1ps = 10^{-12}s$) resolution of the changing magnetic properties of a magnetic multilayer thin film such as CoFe/FeMn. This work and the quest for ultrafast time resolution is motivated by very recently published results. Two papers in particular showed that such ultrafast techniques were effective in probing magnetization changes on a fast time scale; E. Beaurepaire *et al*. [16] measured magnetization changes in ferromagnetic nickel with better than 1ps resolution, and Ganping Ju *et al*. [15] found that magnetization reversal in under a nanosecond was possible.

II. Background and Theory

A. Magnetism and Domains

On an atomic level, individual atoms have magnetic moments that arise due to the orbital angular momentum and the inherent spin of uncoupled electrons in the atom's valence shell. The magnetic behavior of solids depends on the mechanics of how the magnetic moments of individual atoms interact with the magnetic moments of their neighboring atoms and how these individual magnetic moments respond to an applied external magnetic field.

In paramagnetic and diamagnetic materials, there is no exchange force coupling the magnetic moments of individual atoms; the direction of each atom's

magnetic moment is therefore random from one atom to the next. Thus, no net

magnetic moment exists in the absence of external magnetic fields. When an

external magnetic field $\mathbf{H_{ext}}$ is applied to a paramagnetic material, the magnetic

moments of individual atoms experience a torque, resulting in an induced net

magnetic moment in the material proportional to the strength of and in the same

direction as $\mathbf{H_{ext}}$. Applying an external magnetic field to a diamagnetic material

can be visualized classically as causing electrons in the material to change their

velocity so as to oppose the change in magnetic flux supplied by the applied field

[1]. This results in an induced net magnetic moment in the direction opposite of

$\mathbf{H_{ext}}$.

The third broad type of magnetism is fundamentally different. Unlike

paramagnetic and diamagnetic materials, ferromagnetic materials exhibit

exchange coupling between neighboring atoms. This effect is relativistically

quantum mechanical in nature, but suffice it to say that Coulomb repulsion

between electrons is minimized when the magnetic dipoles of neighboring atoms

all point in the same direction [2].   As a result of this coupling, regions of

magnetically aligned atoms, called domains, form spontaneously in ferromagnetic

materials. Until such a material has been subjected to an external magnetic field,

no one direction is preferred, and on a macroscopic scale, the net magnetization

will be approximately zero. But if subjected to an external magnetic field, the

domain structure of the sample will change.

Consider two adjacent domains. Atoms lying in the boundary region

between the two domains, called a domain wall, are in a position of strained

equilibrium; their atomic dipole is pointing in a direction such that the torque supplied by one domain just balances the opposing torque supplied by the other. When an external field is applied, it exerts a torque on all dipoles not aligned with the field. The magnetic dipoles of the domain wall atoms will now rotate and align themselves with the domain which is most aligned with the external field. In this way, domains aligned with the external field will grow at the expense of neighboring domains which are less aligned. Once the external field is sufficiently strong, all magnetic dipoles within the material will be aligned in its direction and the material is then said to be at magnetic saturation. If the field is then turned off, domains will form once again, but this time there will be a net magnetic moment, called the remnant magnetism, in the direction of $\mathbf{H_{ext}}$.

The behavior and structure of these domains gives rise to a ferromagnetic material's characteristic hysteresis curve, a curve describing the net magnetization of the material versus the strength of an applied external magnetic field. In a material lacking domain structure, the net magnetization of the material exhibits a one-to-one correspondence with an applied field. But in a ferromagnetic material, the external field must alter the domain structure in order to change the net magnetization of the material. Thus, the material's magnetization depends upon its previous domain structure, and the net magnetization of the sample is not necessarily uniquely defined for a given external field. When the strength of an applied field is systematically increased and decreased so as to drive a sample to magnetic saturation, first in one direction and then in the opposite direction, the values of sample magnetization versus the applied field will trace out a hysteresis

curve for the sample.

We would like to investigate both the magnetic properties of certain ferromagnetic (FM) thin films and more specifically, how these change on a picosecond time scale as the domain structure is disturbed and then allowed to resettle. We will make use of the magneto-optical Kerr effect (MOKE) to measure the magnetization of a sample, and we will use ultrafast MOKE to study the magnetization as it changes on a picosecond time scale.

B. Magneto-Optical Kerr Effect

The magneto-optical Kerr effect (MOKE) is observed as a net rotation and elliptical polarization of incident vertically linearly polarized light as it is reflected off a magnetized sample [3]. This change in the polarization state, or $\wp$-state, of an incident electromagnetic wave arises due to the interaction of the electric and magnetic fields of the waves with the spin of the electrons in the material. The magnitude of this change in polarization is proportional to the magnetization of the sample. Linearly polarized light can be depicted as a combination of equal amounts of right and left circularly polarized light. Right and left circularly polarized light effectively have different indices of refraction in magnetized media as they are absorbed and re-emitted differentially depending on the direction and strength of the sample's magnetization [4]. The reflected light is then the sum of unequal proportions of right and left circularly polarized light; that is, the reflected light is now elliptically polarized with its axis of polarization

rotated by an amount θ_κ, called the Kerr angle. The Kerr angle is approximately

given by the expression [5]:

$$\boldsymbol{q}_k = -\mathrm{Im}\left(\frac{N_+ - N_-}{N_+ N_- - 1}\right) \tag{1}$$

where N_+ and N_- are the complex propagation velocities of right and left

circularly polarized light, respectively. Thus, by passing this reflected light

through a crossed polarizer, we can pick off the component orthogonal to the

direction of the incident light. By measuring its magnitude as a function of an

external magnetic field applied to the sample, a hysteresis loop for the sample can

be constructed.

When describing polarized electromagnetic radiation, matrices provide a

concise mathematical representation of these $\wp$-states which is readily applicable

to coherent beams. A beam can be represented in terms of its electric field

vector, called a Jones vector after R. Clark Jones who developed the technique in

1941 [6]. Everything about a $\wp$-state can be gleaned from the corresponding

Jones vector, which takes the form

$$\mathbf{E} = \begin{bmatrix} E_{0p}e^{ij_p} \\ E_{0s}e^{ij_s} \end{bmatrix} \tag{2}$$

where φ_p and φ_s are the phases of the horizontal and vertical components of the

beam, respectively[1*]. The geometry of the $\hat{\mathbf{p}}$ and $\hat{\mathbf{s}}$ directions is illustrated in

Figure 1 below.

---

[1] In some mathematical discussions, e.g. Hect and Zajac, *Optics* [6], x and y are used in place of p and s. In experimental applications where a beam is incident on a sample or optical element, $\hat{\mathbf{p}}$ and $\hat{\mathbf{s}}$ are commonly used to refer to the directions (both perpendicular to the direction of propagation) which are parallel and perpendicular to the plane of incidence, respectively.
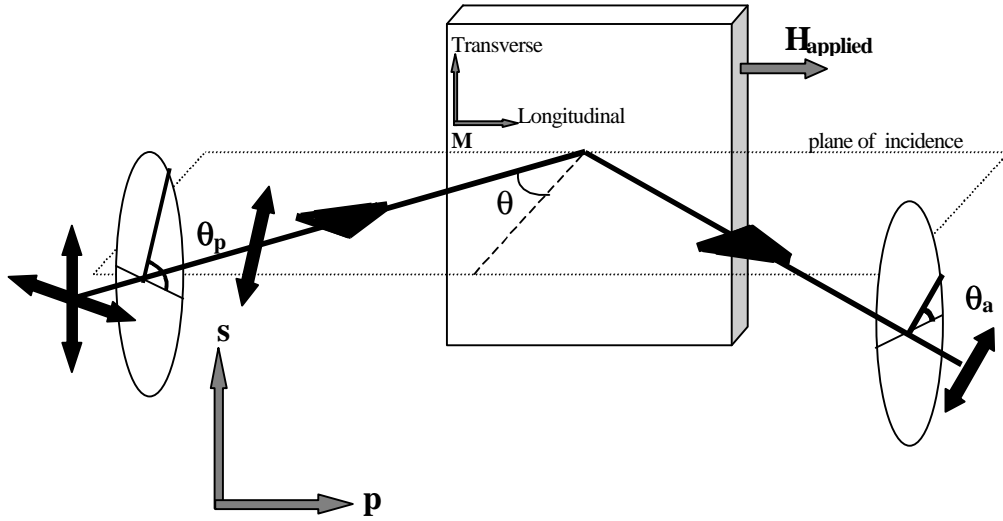
Figure 1: Geometry of reflection off a magnetized sample with magnetization components in the transverse and longitudinal directions. Orientation of the $\hat{\mathbf{p}}$ and $\hat{\mathbf{s}}$ directions is shown, as well as arbitrary polarizer and analyzer angles, θ_p and θ_a respectively. θ is the angle of incidence.

The Jones vector representation yields a convenient means of describing any polarization state. For example, consider a left circularly polarized $\wp$-state. The horizontal and vertical amplitudes are identical, i.e. $E_{0p}=E_{0s}$, and the p-component exhibits a phase lag of $\pi/2$ relative to the s-component. Using the form $(kz - \omega t)$ for the phase as used by Hect and Zajac [6], a phase lag of $\pi/2$ necessitates adding $\pi/2$ to φ_p, yielding

$$\mathbf{E_L} = \begin{bmatrix} E_{0p}e^{i\varphi_p} \\ E_{0p}e^{i(\varphi_p+\pi/2)} \end{bmatrix}. \tag{3}$$

For most applications, specific phase and amplitude information need not be preserved. Then, dividing out the common factor of $E_{0p}e^{i\varphi_p}$ and multiplying by $1/\sqrt{2}$ gives a normalized form of

$$\mathbf{E_L} = \frac{1}{\sqrt{2}}\begin{bmatrix} 1 \\ e^{i p/2} \end{bmatrix} = \frac{1}{\sqrt{2}}\begin{bmatrix} 1 \\ i \end{bmatrix} \qquad \text{and similarly,} \qquad \mathbf{E_R} = \frac{1}{\sqrt{2}}\begin{bmatrix} 1 \\ -i \end{bmatrix}. \qquad (4)$$

The normalized Jones vectors for horizontal and vertical $\wp$-states are, of course,

$$\mathbf{E_h} = \begin{bmatrix} 1 \\ 0 \end{bmatrix} \quad \text{and} \quad \mathbf{E_v} = \begin{bmatrix} 0 \\ 1 \end{bmatrix}. \qquad (5)$$

$\mathbf{E_L}$ is orthogonal to $\mathbf{E_R}$ (i.e. the two vectors are linearly independent: $\mathbf{E_L} \bullet \mathbf{E_R}^* = 0$), and $\mathbf{E_h}$ is likewise orthogonal to $\mathbf{E_v}$. Any $\wp$-state can therefore be described as a linear combination in either the left and right circular $\wp$-state basis or the horizontal and vertical linear $\wp$-state basis.

It is now left to consider how a polarized electromagnetic wave is modified upon encountering an interface. One boundary condition requires the continuity of the electric and magnetic field vectors, **E** and **H,** across any interface [7]. For the case of reflection, this boundary condition dictates the need for a time-independent relation connecting the incident wave, characterized by $\mathbf{E_i}$, to the reflected wave, $\mathbf{E_r}$, for all points on the interface. Thus, $\mathbf{E_i}$ and $\mathbf{E_r}$ must be identical functions of time; namely, they must have identical frequencies ($\omega_i = \omega_r$). Requiring continuity at all points along the interface leads to the well-known relation that the angle of incidence equals the angle of reflection [see Lorraine, *Electromagnetic Fields and Waves* [7], for a more detailed derivation].

The effect of an optical element or interface on the $\wp$-state of an incident beam can be represented by a 2 x 2 matrix, called a Jones matrix. A polarizer set at an angle θ_p relative to the $\hat{\mathbf{p}}$ direction[2], for instance, has the Jones matrix

$$\begin{bmatrix} \cos\boldsymbol{q}_p & 0 \\ 0 & \sin\boldsymbol{q}_p \end{bmatrix}. \tag{6}$$

After an initial beam of amplitude E_0 passes through a polarizer, then, the polarization of the beam incident on the sample is given by

$$\mathbf{E_i} = E_0 \cos\boldsymbol{q}_p\hat{\mathbf{p}} + E_0 \sin\boldsymbol{q}_p\hat{\mathbf{s}} \ . \tag{7}$$

When polarized light is incident upon a magnetized sample, its horizontal and vertical components are modified differentially by the $\hat{\mathbf{p}}$ and $\hat{\mathbf{s}}$ components of the sample's magnetization, $\mathbf{M}$. It becomes convenient, then, to represent the effects of the longitudinal ($M_l\hat{\mathbf{p}}$) and transverse ($M_t\hat{\mathbf{s}}$) components of $\mathbf{M}$ by the 2 x 2 scattering matrices, S^l and S^t, respectively. The polar Kerr-effect, due to magnetization components normal to the surface of a sample, shall not be discussed. The electronic geometries giving rise to such components are energetically unfavorable in magnetic thin films and are generally not observed. Magnetization components in a sample are then restricted to lie in the plane of the sample's face.

Assuming a typical geometry in which the sample is held normal to the plane of incidence as in *Figure* 1 (see *Figure 2* for an experimental MOKE setup),

---

[2] A polarizer's angle θ_p is conventionally defined relative to the $\hat{\mathbf{p}}$ direction (e.g. a horizontal $\wp$-state results from $\theta_p=0°$). Care should be exercised in the laboratory as alternative definitions are sometimes used depending on how the polarizers themselves have been assembled.

the magnetization of the film can be written as a linear combination of $\hat{\mathbf{p}}$ and $\hat{\mathbf{s}}$ components. The net scattering matrix S for reflection off a magnetized sample with a saturation magnetization M_s, and transverse and longitudinal components M_t and M_l such that the reflected wave

$$\mathbf{E_r} = S\mathbf{E_i}, \tag{8}$$

is given by

$$S = m_t^2 S^t + m_l^2 S^l \tag{9}$$

where

$$m_t = M_t/M_s, \qquad m_l = M_l/M_s, \tag{10}$$

$$S^t = \begin{bmatrix} r_{pp}^t & r_{ps}^t \\ r_{sp}^t & r_{ss}^t \end{bmatrix} \text{ and } S^l = \begin{bmatrix} r_{pp}^l & r_{ps}^l \\ r_{sp}^l & r_{ss}^l \end{bmatrix}. \tag{11}$$

and since the magnetization of the sample is restricted to being in the plane of the film,

$$m_t^2 + m_l^2 = 1. \tag{12}$$

The elements of the scattering matrices are known as Fresnel reflection coefficients. The subscript and superscript notation signify, for example, that r_{sp}^l is the coefficient for the longitudinal effect relating the reflected s wave to the incident p wave [8]. Notice then that the diagonal elements, r_{pp} and r_{ss}, are the coefficients signifying how much of the original $\wp$-state is simply reflected, while the off-diagonal elements, r_{ps} and r_{sp}, give rise to the net rotation and elliptical polarization that is the magneto-optical Kerr effect.

For the longitudinal Kerr effect in a magnetized medium with index of refraction n, the Fresnel reflection coefficients are given by

$$r_{pp}^{l} = \frac{(n\boldsymbol{b} - \boldsymbol{b}')}{(n\boldsymbol{b} + \boldsymbol{b}')}, \tag{13}$$

$$r_{ss}^{l} = \frac{(\boldsymbol{b} - n\boldsymbol{b}')}{(\boldsymbol{b} + n\boldsymbol{b}')}, \tag{14}$$

$$r_{ps}^{l} = -r_{sp}^{l} = \frac{\sin \boldsymbol{q} \boldsymbol{b} k_2}{n^2 \boldsymbol{b}'(n\boldsymbol{b} + \boldsymbol{b}')(\boldsymbol{b} + n\boldsymbol{b}')}. \tag{15}$$

For the transverse Kerr effect, they are given by

$$r_{pp}^{t} = \left(\frac{n\boldsymbol{b} - \boldsymbol{b}'}{n\boldsymbol{b} + \boldsymbol{b}'}\right)\left(1 + \frac{k_2 \sin 2\boldsymbol{q}}{n^2(n^2 \cos^2 \boldsymbol{q} - 1) + \sin \boldsymbol{q}}\right), \tag{16}$$

$$r_{ss}^{t} = \frac{(\boldsymbol{b} - n\boldsymbol{b}')}{(\boldsymbol{b} + n\boldsymbol{b}')}, \text{ and} \tag{17}$$

$$r_{ps}^{t} = r_{sp}^{t} = 0 \tag{18}$$

where β=cosθ, β′=[1-(sin²θ)/n²]$^{1/2}$, θ is the angle of incidence as measured from

the sample normal, and κ_2=in²Q [8].[3] All of the quantum mechanical effects

responsible for MOKE —the effectively different indices of refraction for left-

and right-circular ℘-states due to the spin-orbit interaction—are imbedded in the

parameter Q. In the limit of a non-magnetic sample, Q goes to zero, the off-

diagonal elements of S^l which give rise to MOKE disappear, and thus the Fresnel

coefficients become the ordinary Fresnel coefficients for reflection.

Now it is left to determine which polarization components of an incident

beam will contribute to the observed rotation in proportion to the sample's

magnetization. Combining equations (8) and (9) gives

$$\mathbf{E_r} = \left(m_t^2 S^t + m_l^2 S^l\right)\mathbf{E_i}. \tag{19}$$

Using equations (7) and (11) and converting to matrix notation:

$$\begin{bmatrix} E_{r,p} \\ E_{r,s} \end{bmatrix} = m_t^2 \begin{bmatrix} r_{pp}^t & r_{ps}^t \\ r_{sp}^t & r_{ss}^t \end{bmatrix} \begin{bmatrix} E_0 \cos\boldsymbol{q}_p \\ E_0 \sin\boldsymbol{q}_p \end{bmatrix} + m_l^2 \begin{bmatrix} r_{pp}^l & r_{ps}^l \\ r_{sp}^l & r_{ss}^l \end{bmatrix} \begin{bmatrix} E_0 \cos\boldsymbol{q}_p \\ E_0 \sin\boldsymbol{q}_p \end{bmatrix}. \quad (20)$$

Multiplying yields

$$E_{r,p} = \left(m_t^2 r_{pp}^t + m_l^2 r_{pp}^l \right) E_0 \cos\boldsymbol{q}_p + \left(m_t^2 r_{ps}^t + m_l^2 r_{ps}^l \right) E_0 \sin\boldsymbol{q}_p \quad (21)$$

$$E_{r,s} = \left(m_t^2 r_{sp}^t + m_l^2 r_{sp}^l \right) E_0 \cos\boldsymbol{q}_p + \left(m_t^2 r_{ss}^t + m_l^2 r_{ss}^l \right) E_0 \sin\boldsymbol{q}_p. \quad (22)$$

Simplifying using equations (12) and (18) gives

$$E_{r,p} = \left(m_t^2 r_{pp}^t + m_l^2 r_{pp}^l \right) E_0 \cos\boldsymbol{q}_p + m_l^2 r_{ps}^l E_0 \sin\boldsymbol{q}_p \quad (23)$$

$$E_{r,s} = m_l^2 r_{sp}^l E_0 \cos\boldsymbol{q}_p + r_{ss}^l E_0 \sin\boldsymbol{q}_p. \quad (24)$$

If the polarizer angle θ_p is set to 90°, yielding s-polarized incident light, these expressions simplify to

$$E_{r,p} = m_l^2 r_{ps}^l E_0 \quad (25)$$

$$E_{r,s} = r_{ss}^l E_0. \quad (26)$$

The vertical $\wp$-component produced by the longitudinal effect is modified in intensity by r_{ss}^l independently of the sample's magnetization. However, the longitudinal Kerr-effect evidently produces a horizontal $\wp$-component which is proportional to the square of a sample's magnetization. A measurement of the variations in the intensity of this component will therefore provide information about a sample's changing magnetic properties. By directing the reflected beam

---

[3] κ_2 is the off-diagonal of the relative permeability tensor. Q is known as the Voight magneto-optical parameter.

through an analyzing polarizer, the component of interest can be isolated. Using

equation (7), the field transmitted by the analyzer is

$$\mathbf{E_t} = E_{r,p}\cos\boldsymbol{q}_a\hat{\mathbf{p}} + E_{r,s}\sin\boldsymbol{q}_a\hat{\mathbf{s}}. \tag{27}$$

When the angle θ_a is set to $\approx 0°$ or $1°$,

$$E_t \approx E_{r,p}. \tag{28}$$

The signal detected by the photodiode, normalized to the incident intensity, is

seen to be

$$\frac{I}{I_0} \propto \frac{|E_t|^2}{|E_0|^2} \propto \frac{|E_{r,p}|^2}{|E_0|^2} = \left|m_l^2 r_{ps}^l\right|^2 \tag{29}$$

[9]. Substituting equation (15) for r_{ps}^l and assuming n is real gives

$$\frac{I}{I_0} = \frac{M_l^4}{M_s^4}\frac{\sin^2\boldsymbol{q}\cos^2\boldsymbol{q}n^4 Q^2}{n^4(\boldsymbol{b}')^2(n\boldsymbol{b}+\boldsymbol{b}')^2(\boldsymbol{b}+n\boldsymbol{b}')^2}. \tag{30}$$

An experimental setup by J. M. Florczak and E. Dan Dahlberg makes use of this

dependence of intensity on the angle of incidence, θ [8].

C. Nonlinear Optics

Until this point, the polarization response of optical elements and

magnetic samples has been calculated by considering of the element's response to

the electric field associated with an electromagnetic wave; that is, we have

assumed that the response of the medium's atomic system is directly and linearly

proportional to the electric field vector of the electromagnetic wave in question.

This first-order response takes the form

$$\mathbf{P} = \boldsymbol{e}_0 \, c\mathbf{E} \tag{31}$$

where ε_0 is the permittivity of free space and χ is the susceptibility of the medium.

[6, 10, 11] This approximation holds for processes including reflection, refraction, transmission, birefringence, and superposition for low-intensity light. But for processes where high-intensity light such as that produced by a laser is used, the approximation breaks down, as illustrated by the analogy that follows.

Conceptually, the oscillatory response of electrons in an atomic system to an electromagnetic wave can be visualized as being analogous to a classical harmonic oscillator's response to an applied force. While such a spring typically exhibits a restoring force that is linearly proportional to the applied force, the application of a sufficiently large driving force will push the spring beyond its elastic limits, eliciting a non-linear response from the system. In a similar manner, the electrons in a medium fail to respond in a strictly linear fashion when the intensity (or equivalently the amplitude of the electric-field vector) of an incident electromagnetic wave is sufficiently large. A focused beam of laser light can provide the requisite intensity for eliciting such non-linear behavior [11]. The dependence of polarization of electromagnetic waves on the incident electric field is thus seen to posses higher order terms. Equation (31) is therefore replaced by

$$P = P_1 + P_2 + P_3 + \cdots = \boldsymbol{e}_0\left(\boldsymbol{c}_1 E + \boldsymbol{c}_2 E^2 + \boldsymbol{c}_3 E^3 + \cdots\right) \tag{32}$$

where the susceptibility coefficients decrease in magnitude for higher order terms.

Nonlinear effects occur in optical media, most notably in crystals. One phenomenon that results as a consequence of these non-linear terms is that of second harmonic generation.

For an incident electromagnetic wave of frequency ω described by

$E_i\cos\omega t$, the second order polarization term becomes

$$P_2 = e_0\, c_2 E_i \cos^2 wt \tag{33}$$

which can be rewritten, using the identity $\cos2x=\cos^2x-\sin^2x=2\cos^2x-1$, as

$$P_2 = e_0\, c_2 E_i \frac{1}{2}(1 + \cos 2wt), \tag{34}$$

showing that beam resulting from second order effects consists of a DC

component and a component with twice the original frequency [11]. This is

second harmonic generation. A similar phenomenon known as third harmonic

generation also results from the quadratic dependence of P on the electric field

vector.

Second harmonic generation is exhibited by crystals lacking inversion

symmetry[4]. Potassium dihydrogen phosphate (KH_2PO_4, referred to as KDP) is

one such crystal. Crystals with an inversion symmetric axis, such as gallium

arsenide (GaAs), exhibit third-order effects. When two beams are coincident on a

nonlinear crystal, additional nonlinear effects may be observed. In addition to the

second (or third) harmonic generation due to the each beam, a beam dependent

upon the sum or difference of the frequencies of the two original beams may

result. For two beams, P_2 becomes

$$P_2 = \sum_{jk} c_{2,ijk}\, E_j E_k\,, \tag{35}$$

an expression which, when expanded, has terms dependent upon the frequency of

---

[4] A crystal is said to have inversion symmetry if, when the radial coordinate r is replaced with $-r$, its atomic lattice structure does not change, and all physical properties are identical except for a change in sign. In such a crystal, P_2 must be the same as $-P_2$. Because P_2 depends on the *square* of the electric field vector, $P_2=-P_2$ only when $P_2=0$. Consequently, only crystals lacking inversion symmetry exhibit the effects of a second order polarization component [11].

the first beam, the frequency of the second beam, the sum of the two frequencies, and the difference of the two frequencies.

It can be shown that the intensity of such a beam, with frequency $\omega_1+\omega_2$ (which, of course, is just 2ω for incident beams of the same frequency), is maximized when the two beams are matched in phase. That is, intensity is maximized when the wave vector mismatch $\Delta \mathbf{k}=0$. The wave vector mismatch is defined as the difference of the resulting wave vector $\mathbf{k}_s$ from the sum of the two wave vectors, $\mathbf{k}_1$ and $\mathbf{k}_2$, of the original beams, or in symbols

$$\Delta \mathbf{k} = \mathbf{k}_1 + \mathbf{k}_2 - \mathbf{k}_s. \tag{36}$$

When $\Delta \mathbf{k}=0$, the resulting wave vector $\mathbf{k}$ is evidently given by $\mathbf{k}_1+\mathbf{k}_2$; that is, the resulting beam will be seen emerging between the two original beams (see *Figure 3*). In this condition, the two beams are said to be phase matched. In a phase matched condition, the terms in P_2 that depend upon the difference in the two beams frequencies do not contribute; thus the emerging beam is due to the sum of the two frequencies.

The conditions necessary for higher order harmonic generation are extremely sensitive to the alignment of the incident beams with one another and with the crystal. This sensitivity becomes useful in the laboratory, as a higher order transmitted beam will not be observed unless precise alignment of the incident beams is achieved.

III. Experimental Setups and Methods

A.   Linear MOKE

Two detection schemes were employed when using linear MOKE to study

samples. Both setups utilize a 4.7mW maximum power HeNe diode laser, which

emits light in the visible red region (λ=670nm). The laser light passes through a

convex lens, focal length 20cm, to focus the beam, then passes through a Glan-

laser polarizer with θ_p set to 90°, resulting in vertically linearly polarized light.

This polarized light is then effectively pulsed at about 1 kHz by an optical

chopper. The pulsed beam then reflects off the sample situated between the poles

of an electromagnet, which is powered by a computer-controlled Kepco power

supply. Because the distance between the poles of the electromagnet can be

adjusted, a Hall probe next to the sample provides feedback to the computer as to

the actual magnetic field produced by the current supplied. The reflected beam

passes through a second lens, and from this point the two detection methods

diverge.

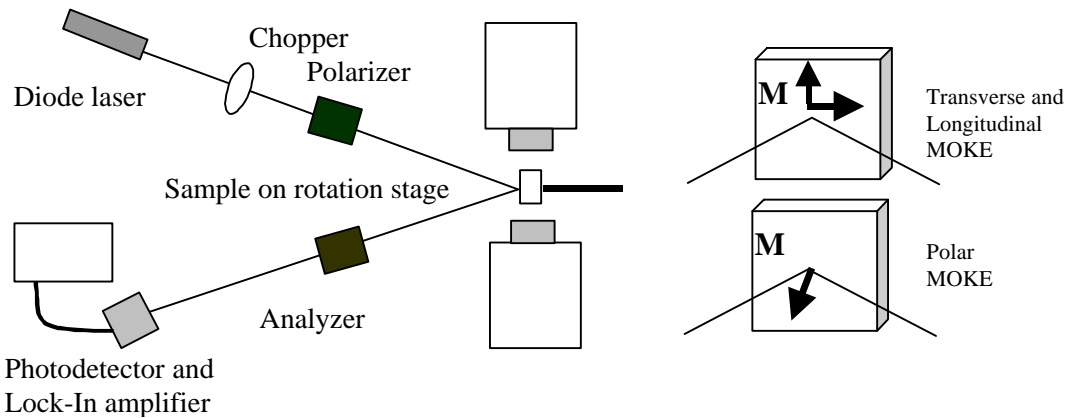The analyzer method is elegant in its simplicity, as illustrated in *Figure 2.*

Figure 2: Linear MOKE setup using the polarizer/analyzer detection scheme.
The reflected beam passes through a second, nearly-crossed polarizer, or analyzer,

with θ_a set to ≈0°. Since the Kerr effect is small, in practice this angle is usually closer to 1° in order to maximize the signal-to-noise ratio [12]. Next, the beam is detected by a photodiode. The signal from the photodiode is then coupled with the measured frequency of the optical chopper through the Stanford SR530 lockin amplifier. The lockin ignores all output from the photodiode except that which is at the same frequency as the optical chopper. In this manner, a signal that would otherwise be drowned out by noise becomes easier to observe. While this setup can provide usable results, it is nevertheless extremely vulnerable to small perturbations, especially any fluctuations in the output power supplied by the laser. The hysteresis loops obtained from this setup are consequently prone to frequent shifts. An alternative detection scheme which accounts for such effects is therefore desirable.

This second detection scheme is inspired by a similar technique utilized by J.J. Baumberg *et al.* in an experiment using ultrafast Faraday spectroscopy to study magnetic semiconductor quantum structures [13]. It was suggested by Paul Crowell of the University of Minnesota. Instead of passing through an analyzer, the reflected beam passes through a half-wave plate set at θ_{hwp}=45°. The Jones matrix for this optical element is given by the product of the Jones matrix for a half wave plate and a 45° rotation matrix:

$$\begin{bmatrix} 1 & 0 \\ 0 & -1 \end{bmatrix} \begin{bmatrix} \cos 45° & -\sin 45° \\ \sin 45° & \cos 45° \end{bmatrix} = \frac{1}{\sqrt{2}} \begin{bmatrix} 1 & 0 \\ 0 & -1 \end{bmatrix} \begin{bmatrix} 1 & -1 \\ 1 & 1 \end{bmatrix} = \frac{1}{\sqrt{2}} \begin{bmatrix} 1 & -1 \\ -1 & -1 \end{bmatrix} \quad (37)$$

This has the net effect of rotating the axis of polarization of the light by 90°+ 45°=135°, or ¾π radians. If, for example, the light entering the half-wave plate

were in a purely linear vertical $\wp$-state, the resultant Jones vector is given by

$$\begin{bmatrix} 1 & -1 \\ -1 & -1 \end{bmatrix}\begin{bmatrix} 0 \\ 1 \end{bmatrix} = \begin{bmatrix} -1 \\ -1 \end{bmatrix} \tag{38}$$

where amplitude factors have been neglected. This is, of course, is the $\wp$-state at 135°.

The resulting beam passes through a Glan-laser (G-L) prism, which anisotropically exhibits different effective indices of refraction for orthogonal linear $\wp$-states. As a result, the vertical and horizontal components of the incident beam are physically separated. Each component is then detected by a photodiode. The signals from these photodiodes are input into a circuit which functions as a differential operational-amplifier (op-amp). The gain of this circuit is given by R_2/R_1. By matching R_1 to R_2, the gain can be normalized to unity, resulting in an output that is just the difference of the two signals [14]. In theory, noise caused by environmental perturbations, e.g. fluctuations in laser intensity, will be canceled when the two signals are subtracted, resulting in enhanced stability of the output sent to the lockin amplifier relative to that of the analyzer method.

In either method, a LabView program written by graduate student Jason Gammon of the College of William and Mary provides a means to coordinate all of the instruments involved in the experiment as well as a simple way to assimilate the data gathered. The program is designed to drive a sample through its hysteresis cycle by increasing and decreasing the strength of the supplied

external magnetic field. The computer has control of the Kepco power supply, and uses feedback from the Hall probe to adjust the current level supplied to the electromagnet until the desired magnetic field strength is attained. Hall probe readings are recorded as x-values and the readings from the lockin amplifier as y-values. After a user-specified time constant, typically 50-350 ms, the program again reads these two values. This process is repeated a specified number of times, typically 10-100 times, per current level. The samples are then averaged and a point plotted, the current level changed by a user-specified increment (0.005-0.020 amps), and the process repeated.

B.   Nonlinear Pump-Probe Methods and Autocorrelation

Measurements of changes in a sample's magnetic properties due to the nonlinear response of its electrons to an external driving force require the introduction of a second beam. The beam used in linear methods is known as the probe beam, its intensity being sufficiently low so as not to disturb a sample's electronic structure. The second beam is called the pump beam and serves as the requisite nonlinear disturbance. Both beams originate from the same source, namely a 1W, 845nm Ti:Saph laser which provides 2ps pulses at 80 MHz and is pumped by a 5W Millennium CW (continuous wave) laser. This source beam passes through a 50% reflective, 50% transmissive mirror, or beam splitter (see *Figure 3*). The pump beam then reflects off a series of static mirrors as it is directed towards the sample. The probe beam enters a retroreflector, an optical device which produces a beam parallel to and in the opposite direction of an

24

incident beam. This retroreflector is mounted on a translation stage, the purpose

of which will provide for various pump-probe delay times. A neutral density

filter attenuates the emerging beam, which then reflects off a series of mirrors,

resulting in a beam parallel to the pump beam. The two beams pass through a

lens, focusing the parallel beams onto a single point coincident with the sample.

On the way to the sample, the probe beam passes through an optical chopper. The

reflected pump beam is dumped, while the reflected probe beam is analyzed via

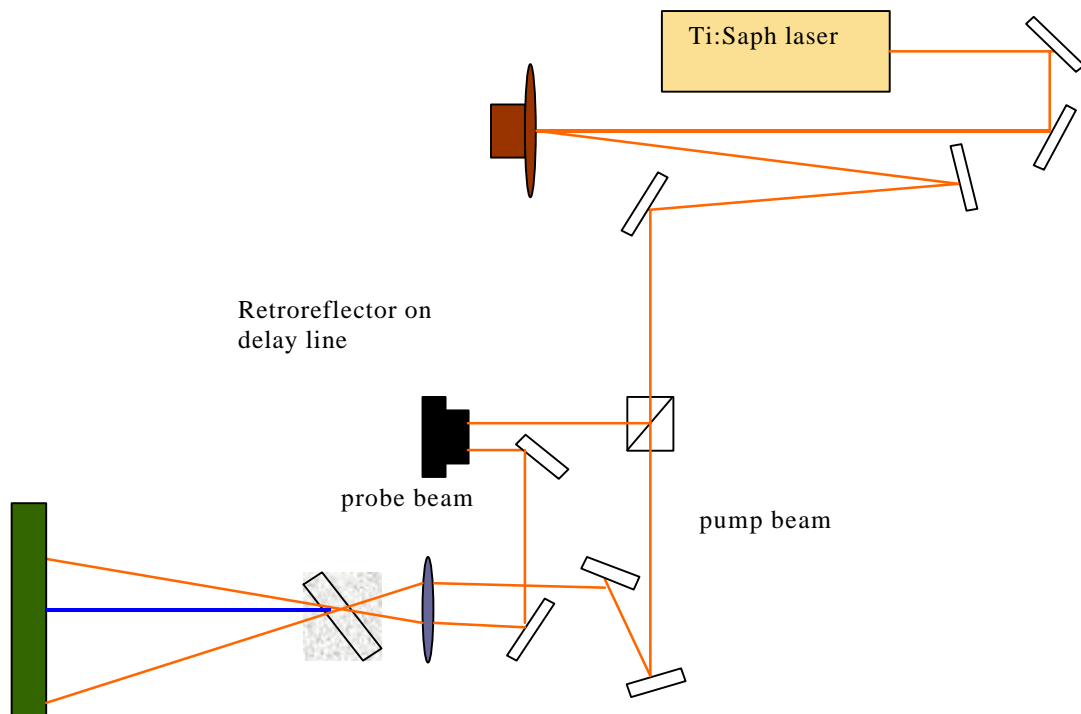one of the detection schemes outlined in the previous section.

Figure 3: Nonlinear setup showing optical delay line. Here, the system is setup for autocorrelation using a KDP crystal.

In order to determine the effect of the pump beam on a real time scale, the probe beam must be probing the same physical region of the sample being hit by the pump beam (i.e. the two beams must be overlapped in space), and the difference in arrival times of the two beams must be known precisely. To this end, the zero-delay point in beam separation (i.e. the condition in which the beams are overlapped in time, arriving simultaneously at the sample's surface) must be determined. Once a zero-delay condition has been achieved, the path length of the probe beam can be increased to provide the desired delay time between the arrivals of the pump and probe beams.

The two beams will arrive at the sample simultaneously when they traverse identical path lengths from the point at which they are separated by the beamsplitter. The path lengths should be matched to within a millimeter before securing the translation stage, set to neutral to allow maximum travel in both directions, to the lab table.   Fine-tuning of the mirrors and first lens is then required to achieve beams that are focused on the surface of the sample, and that are precisely overlapped in space. From this point, two different methods were used to determine when the zero-delay condition had been reached.

The first method makes use of the nonlinear properties of a KDP crystal. If the two incident beams are both overlapped and phase-matched, a beam of twice the frequency should be seen emerging between the two transmitted beams (again, refer to *Figure 3*). The incident beams originate from our Ti:Saph laser and are in the visible red region with a wavelength of $\lambda=845$nm. A beam resulting from the sum of their frequencies will therefore have half the

wavelength, or 423nm, which is in the visible violet region. This is convenient, as the desired beam can be detected with the unaided eye. However, the thickness of the KDP crystal in this setup is approximately one centimeter, which creates an interesting difficulty.

Due to dispersion, that is, the increase of the index of refraction in a medium for increasing frequencies, an electromagnetic wave of frequency 2ω travels through the crystal at a different speed than the beams with frequency ω. Thus, beams which are phase matched upon entering the crystal are out of phase with one another upon exiting the crystal! This difficulty can be overcome in one of two manners.

One solution is to use a crystal which is sufficiently thin that the differences in indices of refraction for different frequencies are negligible for the short time the beams are in the medium, i.e. on the order of 20λ [6]. This solution is relatively impractical, as such crystals are both fragile and costly to manufacture.

A second solution, known as angle tuning, takes advantage of the birefringent properties of a crystal, that is, the dependence of refractive index upon the orientation of an incident electromagnetic wave's polarization direction relative to the optic axis of the crystal. Using the phase matching condition of equation (36), one can solve for the angle θ, between the optic axis of the crystal and the propagation vector of the incident light, at which the indices of refraction for the ω and 2ω beams are precisely equal [10]. For KDP, the intensity of the

transmitted second-harmonic beam exhibits a sharp peak at an orientation corresponding to θ=55° [6].

Once the two beams appear to be focused and overlapped on the crystal, the translation stage should be moved forwards and backwards, and fine adjustments made in the mirrors, until the sum-frequency beam is observed and maximized. To ensure that the observed violet beam is not merely the SHG beam for one of the incident beams, one should verify that alternatively blocking the pump and probe beams eliminates the signal. The intensity of the resulting beam is fairly low; the conversion efficiency of KDP in converting incident beams into a sum-frequency beams has a theoretical maximum of around 20% [6]. A photomultiplier can therefore be positioned so as to detect the SHG beam. Data are then taken in the form of signal voltage versus micrometer reading on the translation stage. The point at which this voltage is maximized is the zero-delay point.

A second method for determining this zero delay setting utilizes gallium-arsenide (GaAs) in place of KDP. Whereas SHG in KDP is a second-order effect, GaAs is inversion-symmetric, and the nonlinear effects it exhibits are third-order. Even so, obtaining a signal from GaAs is typically less problematic than obtaining a signal from KDP, as it is less sensitive to the orientation of the film relative to the incident beam. To obtain a signal dependent upon both beams, the pump beam is chopped at an arbitrary frequency, typically around 1kHz. After being transmitted through the GaAs film, the pump beam is dumped. The probe beam is detected by a photodiode, and the signal sent to the lockin amplifier. The lockin

is triggered by the signal from the optical chopper, rejecting anything not at this reference frequency. As long as the two beams are not overlapped, no interference phenomena will be evident, and hence no part of the signal from the probe will depend upon the chopped frequency of the pump beam. The pump beam effectively alters the local absorption coefficient of the film , and when the two beams are overlapped, we will measure this as a change in the intensity of the transmitted probe beam.

The signal measured by the lockin is expected to be zero so long as the probe beam leads the pump beam. A sudden jump in intensity is expected just beyond the phase-matched condition, followed by an exponential decay of the signal as the probe beam begins to lag the pump. Qualitatively this seems reasonable: in the case of a leading probe beam, the perturbing pump beam has not yet arrived when the probe takes its "snapshot," a slightly lagging probe is witness to the most perturbed state of the system, and a lagging probe sees only remnant effects of the perturbation as the system settles back into its unperturbed state. A quantitative description of this effect can be found in Boyd [10], but is beyond the scope of this paper.

C.   Nonlinear MOKE

Nonlinear MOKE differs from linear MOKE in that the characteristic magnetic properties of the sample under scrutiny are altered by the introduction of a nonlinear perturbing force, namely, the pump beam. The probe beam simply fulfills the role played by the solitary laser in linear MOKE detection schemes.

Stated simply, the pump beam alters the magnetic properties of a sample, and the probe beam then measures these magnetic properties.

The first portion of the setup is identical to that used in autocorrelation (see *Figure 3*), where the crystal is replaced by the sample to be characterized. The second portion of the setup can be either detection scheme described in section III.A., (see *Figure 2*) with the mere addition of a beam dump for the probe beam once it reflects off the sample. Once the zero-delay point has been established using one of the methods outlined in the previous section, the translation stage can be moved to provide various pump-probe delay times. By systematically varying the strength and direction of an external magnetic field, "snapshots" of the magnetic properties of the sample in the form of hysteresis loops can be constructed for a given pump-probe delay time. These snapshots can then compared to those taken for alternate delay times, revealing the time-varying effect of the probe beam on the sample.

One class of thin films of especial interest in the utilization of pump-probe methods is that of exchanged-biased films. An exchange-biased film is characterized by adjacent ferromagnetic (FM) and antiferromagnetic (AF) layers. Antiferromagnetic compounds possess a lattice structure whose exchange interaction is such that within a layer, atomic dipoles align as in a ferromagnetic material, but adjacent layers will align in the antiparallel direction. Evidently, antiferromagnetic materials exhibit a net magnetization of zero. At a ferromagnetic/antiferromagnetic interface, spin-orbit coupling between the two layers determines a preferred direction of alignment (i.e. a splitting of the energy

states) for the ferromagnetic layer. In this way, the AF layer "pins" the adjacent FM layer in a certain direction. Hysteresis loops characterizing exchange-biased films therefore reveal an effective exchange bias field (a horizontal offset), resulting from external fields applied parallel to and antiparallel to the easy/pinned direction.

The quantum-mechanical nature of the spin-orbit interaction responsible for the pinning at the AF/FM interface is poorly understood [15]. The effect of a pump beam incident on the sample is therefore described phenomenologically as an effective heating of the interfacial electrons, which momentarily imparts to them enough energy to overcome the exchange coupling. Experiments done by Ganping Ju and A.V. Nurmikko *et al*. have specifically investigated the so-called "unpinning" effect of a pump beam on exchanged-biased films, and the corresponding response of the magnetization of the ferromagnetic layer (called ultrafast switching) when the external field is antiparallel to the easy direction of magnetization [15].

The ultimate goal of nonlinear, pump/probe methods is gleaning a comprehensive understanding of the real-time dependence of a sample's changing magnetic properties. This understanding is crucial for technological pursuits including a reduction in the time required for the reading and writing of magnetic-bit data, and an increase magnetic-bit data storage densities.

D. Samples

In all, three thin films were characterized in the course of this project. Two of these films consist of a single ferromagnetic layer and the third is a ferromagnetic/antiferromagnetic/paramagnetic multilayer.

One unpinned ferromagnetic film consists of a single 40nm thick layer of cobalt-iron (CoFe) grown on a silicon substrate. The CoFe was deposited via sputtering. The second is simply 35nm of cobalt (Co), also deposited onto a silicon substrate by sputtering.

Our exchange-biased, or "pinned," film consists of 5nm of niobium (Nb) atop a 40nm ferromagnetic layer of cobalt-iron (CoFe), an 8nm antiferromagnetic layer of iron-manganese (FeMn), a 10nm paramagnetic layer of copper (Cu) and another 250nm of Nb, all grown by sputtering onto a silicon substrate. The top 5nm layer of Nb is intended to protect the underlying layer of CoFe.

IV. Results

A. Autocorrelation

Data were recorded in the form of voltage from a photomultiplier tube versus micrometer reading on the translation stage. The data points were plotted and fit with a Gaussian curve as displayed in *Figure 4*. The micrometer setting corresponding to the maximum of this curve (m2) was defined to be the zero-delay setting. Micrometer settings were then converted into delay time ($3x10^{-4}$m corresponds to 1ps). The full width/half max is used as the definition of pulse width for the laser. In this case, the pulse width for the Ti:Saph laser was measured to be ≈1.8ps.

Autocorrelation

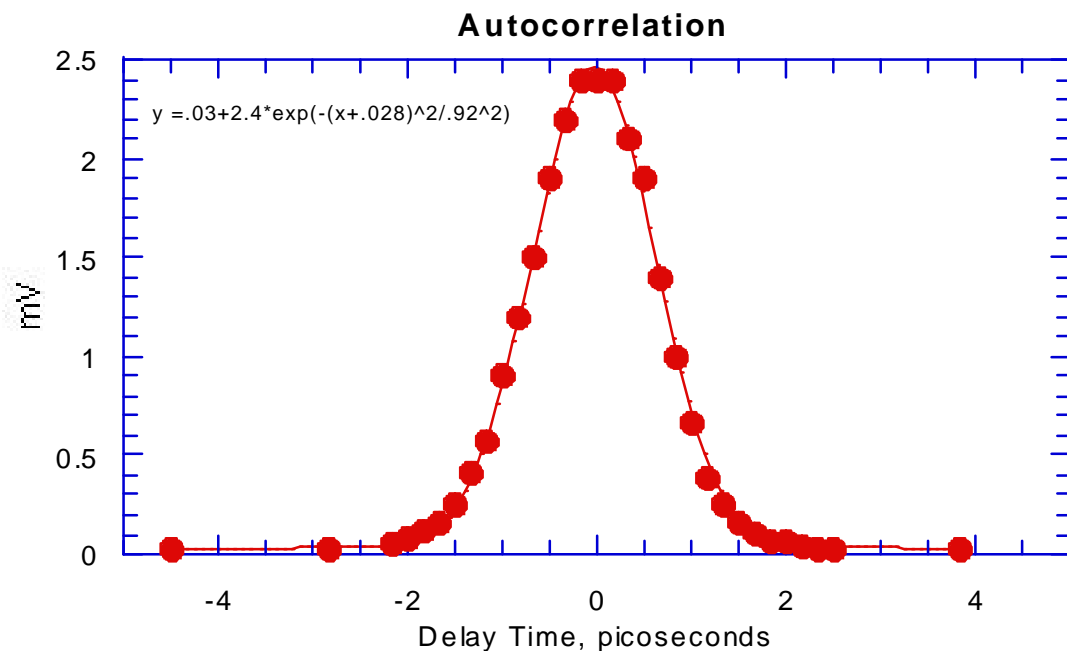$$y = .03+2.4*exp(-(x+.028)^2/.92^2)$$

(mV vs. Delay Time, picoseconds)

Figure 4: Measurement of pulse width of Ti:Saph pulsed laser beam as well as a determination of the zero-delay position of the translation stage using autocorrelation via sum-frequency second harmonic generation in a KDP crystal. The equation of the Gaussian curve that was fit to the data is shown. The pulse width of each laser pulse, identified by the full width of the fitted curve at half its maximum value was calculated to be 1.83918 ± 0.021762 ps.

B. Pump-Probe Differential Transmission through GaAs

Data were recorded in the form of voltage versus micrometer setting on the translation stage. Distance data were converted to probe lag time relative to the zero-delay time. The shape of the resulting plot, shown in *Figure 5*, deviated substantially from that which was expected.
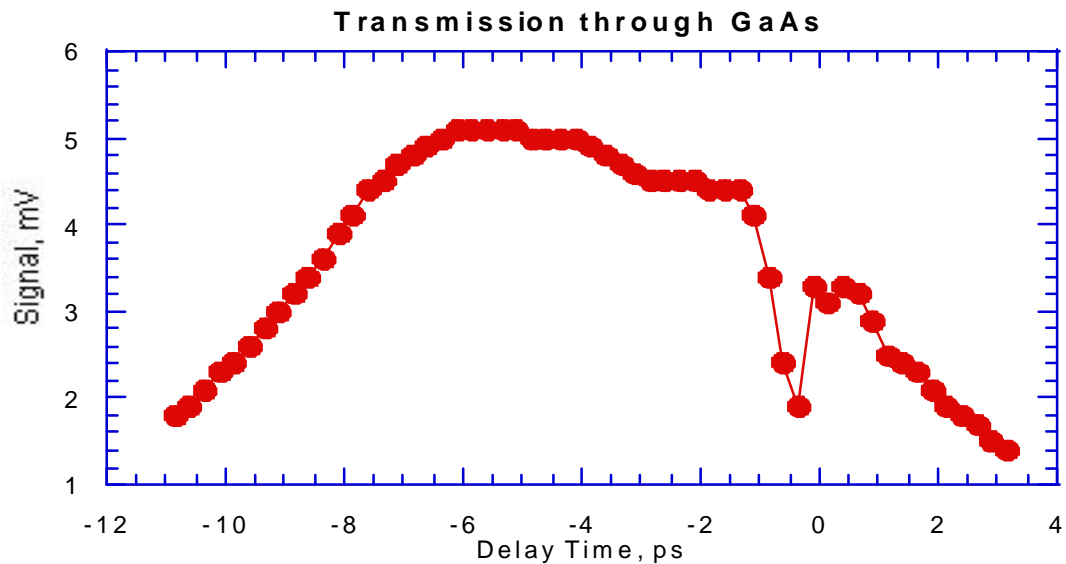
Figure 5: Measurement of differential pump/probe transmission through GaAs with λ=845nm, below the exciton resonance of λ_{ex}=853nm, showing a spike near the zero-delay point.

Upon examination, it was found that the wavelength of the light emitted by the Ti:Saph laser was λ_{actual}=845nm. This was unfortunately below the exciton resonance of λ_{er}=853nm for this GaAs multilayer,. Previous data taken by Chad Weiler using the same laser when λ_{actual} was very near λ_{er} produced a graph of the expected characteristic shape as shown in *Figure 6* [2].
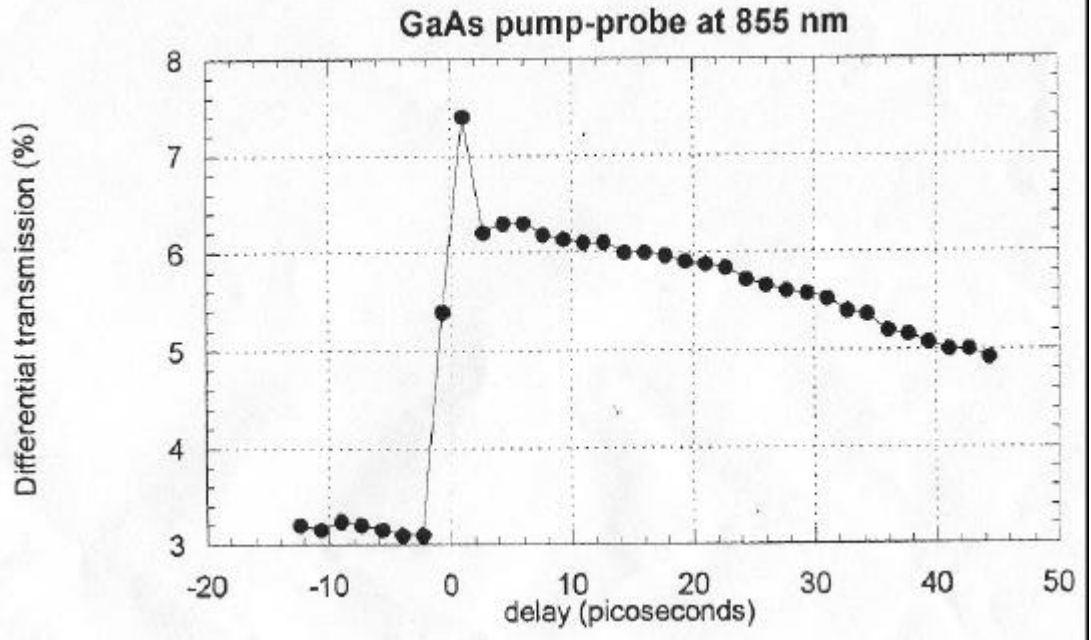
Figure 6: Measurement of differential pump/probe transmission through GaAs with the laser at λ=855nm, near the exciton resonance of λ_{ex}=853nm. As expected, the signal is extremely small for negative delay times (i.e. delays for which the probe pulse arrives at the sample before the pump pulse), a sharp change in transmission occurs near the zero-delay point, and the signal decays for increasing probe delay times.

The non-zero signal obtained here with a probe lead was likely due to thermal heating effects. A downward spike was nevertheless evident at the zero-delay point. In theory, the transmitted signal should be precisely zero for a perfectly phase-matched condition. It appears that the cancellation of the signal near the phase-matched condition managed to overpower the suspected thermal effects.

C. Linear MOKE with Diode Laser

A hysteresis curve obtained for 35nm of cobalt using a single beam from a diode laser exhibits the features typical of unpinned samples as shown in *Figure 7.* The curve is centered around zero-field, revealing the film's lack of magnetic anisotropy (in the direction of the external field). The coercive field is measured at $H_c \approx \pm 160$ Gauss. Saturation magnetism M_s is reached at an eternal field of $\approx \pm 250$ Gauss. The curve is somewhat S-shaped, lacking a sharp flipping of domains at the coercive field. This is evidence of the survival of some domain structure in the film; i.e. the remnant magnetization M_r at zero field, H=0, is less than the saturation magnetism.
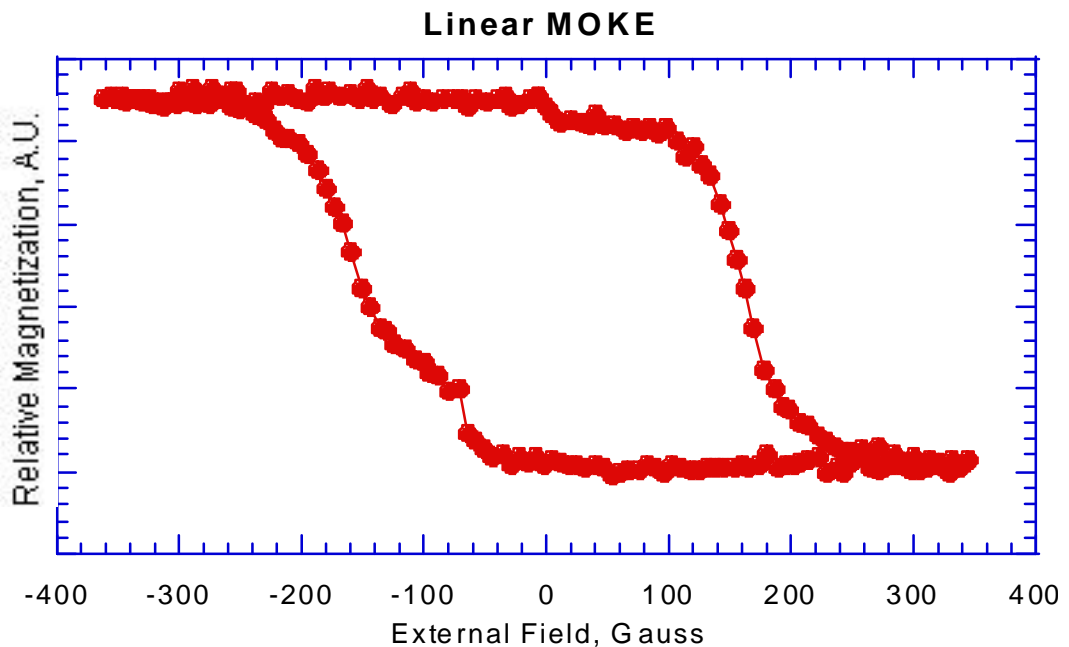

Figure 7: A hysteresis loop generated by 35nm of Co using a HeNe diode laser. Relative magnetization is given in arbitrary units (A.U.).

D. Linear MOKE with Ti:Saph

Features characteristic of films with a magnetic anisotropy along the direction of the applied external field are exhibited by a hysteresis loop obtained for a 40nm thin film using the Ti:Saph laser. *Figure 8* displays data taken using the polarizer/analyzer detection scheme while *Figure 9* displays data for the same sample taken using the half-wave plate/G-L prism detection scheme.

Both curves are nearly centered about zero. Both loops are fairly square, exhibiting an abrupt flipping of domains at the coercive fields of $\approx +22, -31$ Gauss, and. $\approx +22, -38$ Gauss, respectively. This squareness is evidence of permanent alteration of domain structure; the remnant magnetization M_r at zero field is essentially the saturation magnetization, M_s.

The data for the two loops were not taken consecutively, and no comparison of the relative optical alignment precision for the two different schemes was made. Therefore, the apparent greater clarity of data displayed in *Figure 8* as compared to that of *Figure 9*'s data does not constitute a demonstration of the superiority of one detection scheme over the other. Rather, both curves represent the clearest signal obtained on a given day with given laboratory conditions.

One likely source of error in the half-wave plate/G-L prism method lies in the differential op-amp circuit. A little research into differential op-amp circuits revealed that precise resistor matching, to within, $\pm 0.01\%$, is necessary to obtain an acceptable same-mode cancellation [Horowitz]. While all of the resistors used were labeled 100kΩ, their actual resistances were not measured.
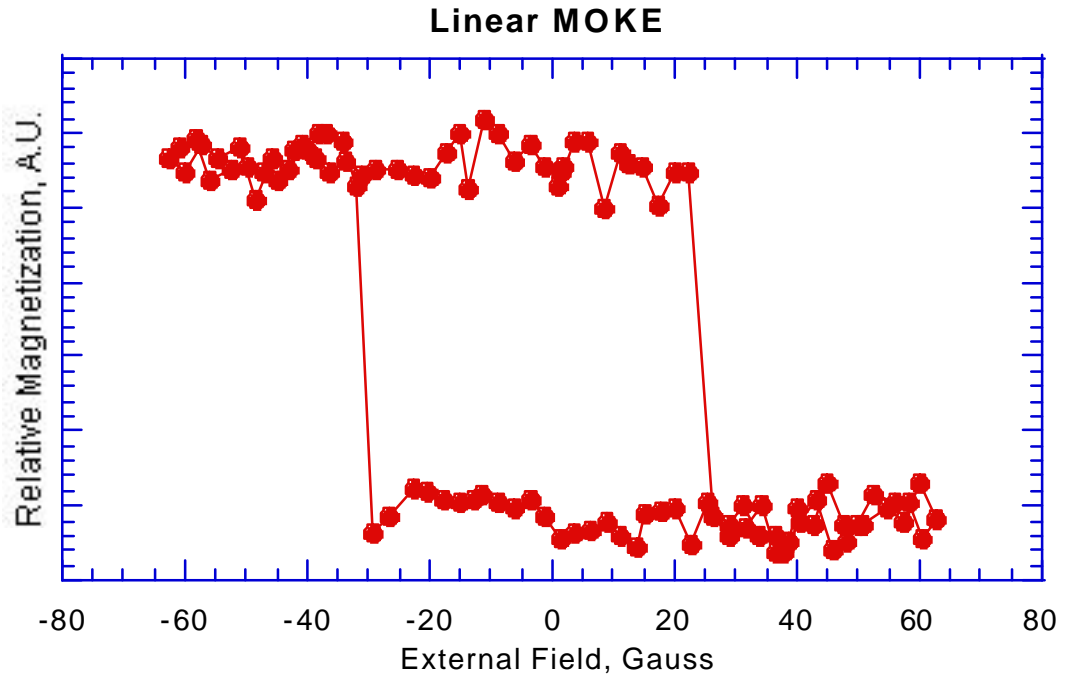
Linear MOKE

Figure 8: A hysteresis loop generated by a 40nm CoFe thin film using a Ti:Saph laser and the analyzer/polarizer detection scheme. Relative magnetization is given in arbitrary units (A.U.).
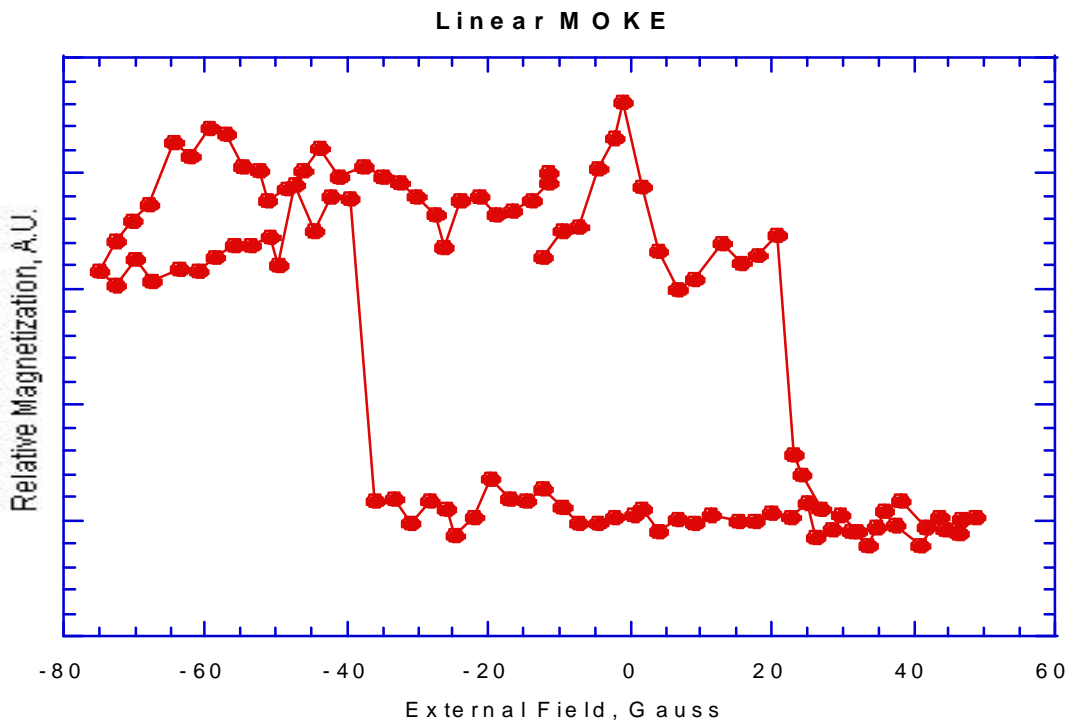
Linear M O K E

Figure 9: A hysteresis loop generated by a 40nm CoFe thin film using a Ti:Saph laser and the half-wave plate/G-L prism detection scheme. Relative magnetization is given in arbitrary units (A.U.).

E. Nonlinear MOKE on CoFe film

Although a clear signal from CoFe using the Ti:Saph laser could not be obtained, the data that were obtained nevertheless seem to demonstrate the effect of a pump beam on the magnetic properties of the film (see *Figure 10* and *Figure 11*). Data for the probe-only condition is graphed with circular markers. The hysteresis loops are once again nearly centered about zero, if somewhat less convincingly. The coercive field is roughly $H_c=\pm50$ Gauss. The graphs are fairly square, with $M_r\approx M_s$. The probe lagged the pump beam by approximately 19.6 ps.

The primary effect of the pump beam appears to be a net reduction in the sample's magnetization, an imposed maximum level of magnetization. This could be explained qualitatively as a consequence of the heating supplied to the material's electrons. The added energy of such heating would prevent the complete alignment of electronic spin states, i.e. it would reduce the maximum possible saturation magnetization.

Curiously, the observed effect of the pump would appear to be more pronounced for magnetization in the negative H direction. The difference in the pump-probe and probe-only curves seemed at first to be noise, a consequence of the poor signal quality. This remains a possibility, although several consecutive runs, alternating between pump and no-pump conditions, appeared to show the same phenomenon. An attempt was made to demonstrate the dependence of the signal on both pump and probe beams. The pump and probe beams were chopped at different frequencies, and we looked for a signal at either the frequency of the pump, or at a sum or difference frequency of the two chopped frequencies. No

such signal was conclusively observed. Therefore, the significance of the data in
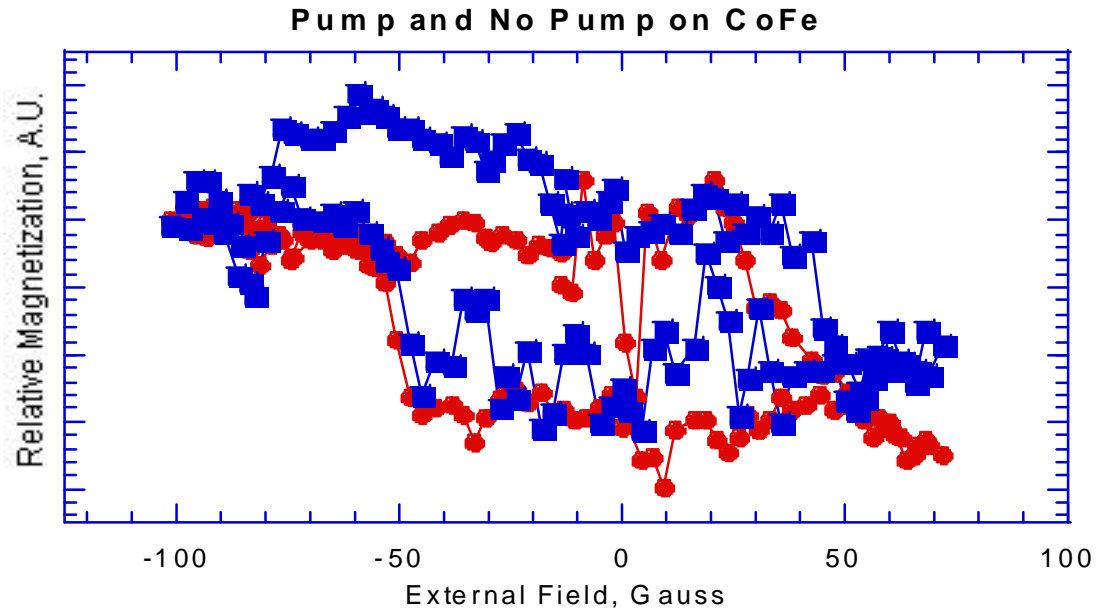
Figure 10 and *Figure 11* is questionable.

Pump and No Pump on CoFe

Figure 10: Hysteresis loops taken with the probe alone (blue squares), and with the pump and probe together for ≈19.6ps probe delay time (red circles). Relative magnetization is given in arbitrary units (A.U.). The trend, a apparent suppression of magnetization, is in the expected direction as in the results of E. Beaurepaire *et al*. [16].
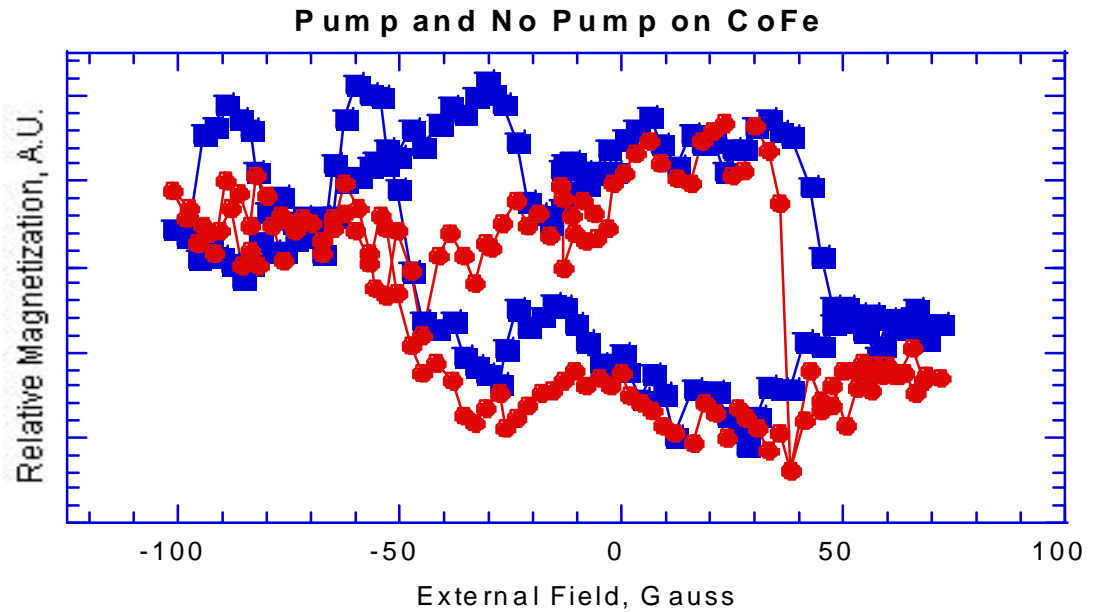
Pump and No Pump on CoFe

Figure 11: A second set of hysteresis loops taken with the probe alone (blue squares), and with the pump and probe together for ≈19.6ps probe delay time (red circles). Relative magnetization is given in arbitrary units (A.U.).

F. Nonlinear MOKE on exchange-biased FeMn/CoFe film

The nonlinear MOKE signal obtained from the exchange-biased

FeMn/CoFe film using the Ti:Saph laser demonstrates the most convincing

evidence for the perturbing effect of the pump beam on the magnetic properties of

the film.

As expected for the exchange-biased film, the curves exhibit an effective

exchange field of $H_{ex} \approx 55$ Gauss, again in the +H direction. The curves are very

nearly square, with $M_r \approx M_s$. But the most interesting feature of *Figure 12* is the

demonstrated vertical shift in the hysteresis curves for the sample when the pump

beam is incident upon the sample. The probe lag time for these curves is
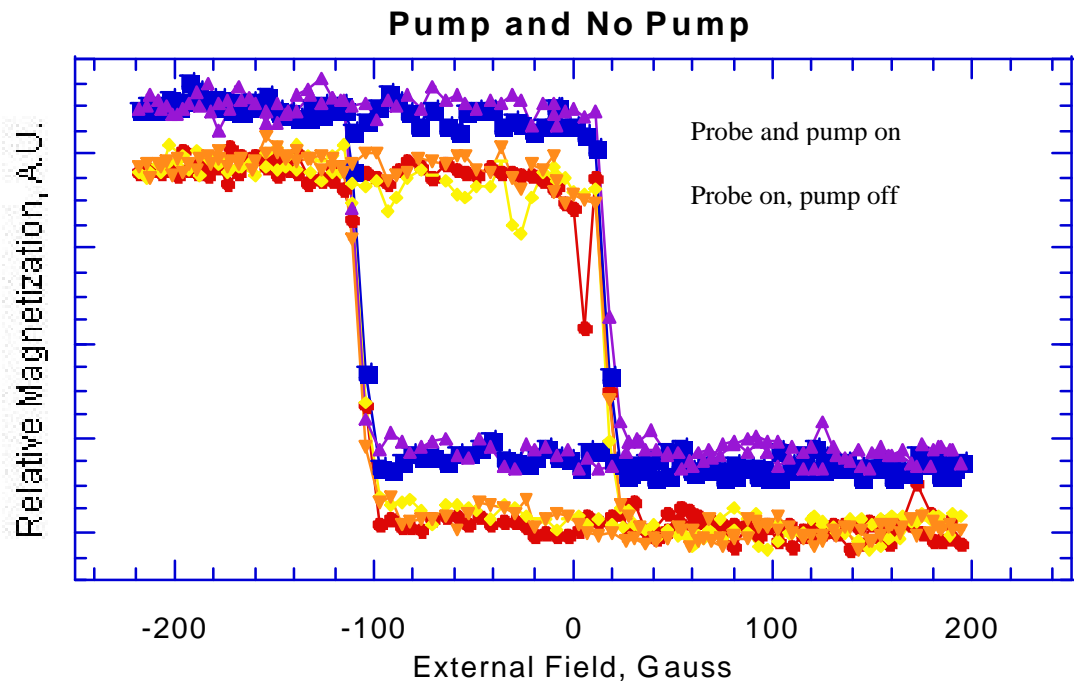
approximately 19.6ps.

Figure 12: Five hysteresis loops taken consecutively on an exchange coupled FeMn/CoFe multilayer film, alternating between probe-only (red circles, orange inverted triangles, and yellow diamonds) and pump and probe with ≈19.6ps probe delay time (blue squares and purple triangles). Relative magnetization is given in arbitrary units (A.U.). While the probe is evidently having an effect, the loops do not exhibit a *downward* shift, nor a change of shape as in the results of E. Beaurepaire *et al*. [16].

41

V. Conclusions and Future Directions

While we were encouraged to measure an apparent hysteresis shift when a pump beam was incident on the FeMn/CoFe film as compared to the hysteresis curves taken in the absence of a pump beam, the cause of the observed shift cannot conclusively be attributed to an actual change in the magnetization of the properties. The pump beam evidently induced the measured change in the intensity of the signal. However, this change could have been due to a mere change in the sample's reflectivity, resulting from heating effects of the pump.

One cause for skepticism arises when these data are compared to the results of E. Beaurepaire, J. –C. Merle *et al*. in their study of ultrafast magnetization changes in ferromagnetic nickel. Their data show a downward shift as well as a shrinking and change in shape of the hysteresis loops from a probe-only condition to a delay time of 2.3ps between the pump and probe pulses [16]. The results of Ju and Nurmikko, *et al*. also show a downward shift, shrinking and change in shape of the hysteresis loops obtained for positive delay times. In contrast, our data show an upward shift with no change in the shape of the hysteresis loops for a 19.6ps delay time. This suggests a different causal connection between each pump pulse and the observed change in intensity of the measured signal than the change in magnetization measured by previous experiments.

A method similar to that used in searching for a signal from GaAs should be added to the experimental setup. The pump and probe beams should be chopped at different frequencies, f_1 and f_2. All signals which seem to evidence a

change in sample magnetization characteristics due to the perturbation of the pump beam should then be tested; if either a probe signal at the pump beam's frequency, or a signal dependent upon the sum frequency $(f_1 + f_2)$, or difference frequency $(f_1 - f_2)$ is observed, the measured changes in signal intensity can be safely attributed to true pump-induced changes in the sample's magnetization. Ju and Nurmikko *et al.* successfully utilized this technique in their study of ultrafast pump-induced magnetization changes in AF/FM pinned (exchange coupled) films [15].

The half-wave plate/G-L prism detection scheme deserves further exploration. Not only does it eliminate one of the extremely sensitive (i.e. difficult to align) G-L polarizers, it also should cancel changes in the measured signal intensity that arise due to fluctuations in laser power. Measuring and carefully matching the actual resistivities of the four resistors in the op-amp circuit should result in a noticeable improvement of the observed signal.

Improvements in laser power are also needed. Although the output power of the pulsed Ti:Saph laser was very close to 1W, measurements of the intensity of the pump and probe beams just before they were incident on the sample revealed the power of the pump beam to be 120mW, and the probe beam to be a mere 6mW. This drastic decrease in power results from the absorption and scattering of laser light by each optical element. A setup with fewer optics is therefore desirable. Fewer optics also characterize a setup which is simpler to align. Additionally, better (i.e. more expensive!) optics would also contribute to a smaller loss in power.

Hysteresis loops should be taken with various pump-probe pulse delay times for each sample. These data can then be compared to gain an understanding of the changes induced by the pump beam in the sample. The relatively short travel in the translation stage used in the nonlinear setups limits the range of possible pump/probe delay times to approximately 45 ps. Although the largest changes in magnetization have been found to occur for pump-probe delay times of 0-3ps [16, 15], the comparatively long relaxation times observed by Ju and Nurmikko *et al*. [15] were on the order of 200ps. A longer translation stage which could provide this order of delay times would allow for a more thorough investigation of the time varying magnetization changes caused by a pump beam.

Eventually, various films should be characterized using the improved ultrafast setup. Once data for multiple samples has been obtained, the properties of these samples can then be compared to determine the advantages and disadvantages of the utilization of any film in a given application relative to the others (e.g. magnetic hardness, coercive field, switching time, saturation magnetization, durability, availability, cost, biocompatibility, etc.). As techniques for measuring magnetic properties of ferromagnetic thin films are improved, and as the fundamental nature of magnetic behavior is better understood, technological applications and advancements are sure to follow closely behind.

VI. References

[1] Tipler, P.A. *Physics for Scientists and Engineers*. 3rd ed. New York: Worth Publishers, 1991.

[2] C. Weiler, "Ultrafast Magnetooptical Kerr Effect." Moravian College, Bethlehem, PA: Unpublished (1999).

[3] P. N. Argyres, Phys. Rev. **97** (1954) 334.

[4] S.D. Bader, Journal of Magnetism and Magnetic Materials **100** (1991) 440-454.

[5] R.M.A. Azzam and N.M. Bashra, "Ellipsometry and Polarized Light" (North Holland, Amsterdam 1977) p. 33.

[6] Hect, Eugene and Alfred Zajac. *Optics*. Reading, Massachusetts: Addison-Wesley Publishing Company, 1979.

[7] Lorrain, Paul and Dale Corson. *Electromagnetic Fields and Waves*, 2nd ed. New York: W. H. Freeman and Company, 1970.

[8] J. M. Florczak and E. Dan Dahlberg, J. Appl. Phys. **67**, 7520 (1990).

[9] Huard, Serge. *Polarization of Light*. Gianni Vacca, trans. Chichester: John Wiley and Sons, 1997.

[10] Boyd, Robert W. *Nonlinear Optics*. Boston: Academic Press, Inc., 1992.

[11] Pedrotti,, Frank L., S. J. and Leno S. Pedrotti. *Introduction to Optics*, 2nd ed. Englewood Cliffs, New Jersey: Prentice Hall, 1993.

[12] J. Gammon, "Magneto-Optical Kerr Effect." College of William and Mary, Williamsburg, VA: Unpublished (1999).

[13] J. J. Baumberg, S. A. Crooker, D. D. Awschalom, *et al*., Phys. Rev. B **50**,

7689 (1994).

[14] Paul Horowitz and Winfield Hill. *The Art of Electronics*. New York:

Cambridge University Press, 1989.

[15] Ganping Ju, A. V. Nurmikko, *et al*. Phys. Rev. Letters **82** (1999) 3705.

[16] E. Beaurepaire, J. -C. Merle, A. Daunois, and J. -Y. Bigot, Phys. Rev.

Letters, **76** (1996) 4250.